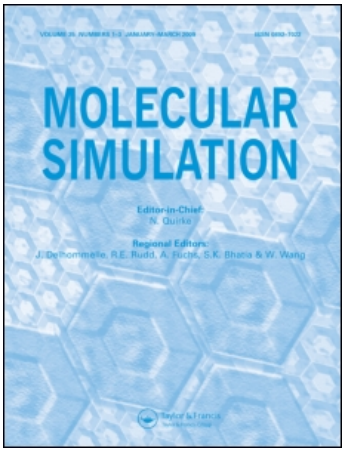

Molecular Simulation
Publication details, including instructions for authors and subscription information:
http://www.informaworld.com/smpp/title~content=t713644482

Density functional theory calculations of ^{11}B NMR parameters in crystalline borates

Sabyasachi Sen[a]
[a] Department of Chemical Engineering and Materials Science, University of California at Davis, Davis, CA, USA

To cite this Article Sen, Sabyasachi(2008) 'Density functional theory calculations of ^{11}B NMR parameters in crystalline borates', Molecular Simulation, 34: 10, 1115 — 1120
To link to this Article: DOI: 10.1080/08927020802258716
URL: http://dx.doi.org/10.1080/08927020802258716

Molecular Simulation
Vol. 34, Nos. 10–15, September–December 2008, 1115–1120

Taylor & Francis
Taylor & Francis Group

Density functional theory calculations of ^{11}B NMR parameters in crystalline borates

Sabyasachi Sen*

Department of Chemical Engineering and Materials Science, University of California at Davis, Davis, CA, USA

(*Received 31 January 2008; final version received 9 June 2008*)

The ^{11}B nuclear magnetic resonance (NMR) shielding and electric field gradient parameters for several borate crystal structures have been calculated using density functional theory and the gauge-including projector augmented wave method with plane-wave basis sets and pseudopotential approximation. The results show good agreement with the existing experimental data. Significantly large variation in the ^{11}B NMR isotropic chemical shift is observed for BO_3 sites with all three bridging oxygen atoms in triborate and boroxol rings and non-ring geometries. Such variations could be attributed to the corresponding differences in the B—O—B angles. The nature of the boroxol rings in glassy B_2O_3 is discussed in light of these data.

Keywords: B-11 NMR; chemical shift; electric field gradient; density functional theory; borate; CASTEP

1. Introduction

Borate crystals and glasses are an important class of materials that have received much attention because of their wide-ranging importance in technological processes, including extensive use in the areas of optics, display and telecommunication [1–3]. The fundamental understanding of these materials and formulation of accurate predictive models for the compositional dependence of physico-chemical properties require detailed knowledge of their atomic scale structure and the dynamical phenomena they exhibit, including transport and relaxation. High-resolution ^{11}B nuclear magnetic resonance (NMR) spectroscopy has played an important role in elucidating the short-range structure around B atoms in a wide variety of borate crystals and glasses [4–10]. The natural abundance of the ^{11}B isotope is $\sim$80% and it is a highly NMR sensitive quadrupolar (nuclear spin $I = 3/2$) nuclide with a relatively large gyromagnetic ratio. Boron atoms in borates are either three- or four-fold coordinated to oxygen atoms, forming BO_3 planar triangles or BO_4 tetrahedra, respectively. The B sites in planar BO_3 triangles are characterised approximately by C_3 symmetry and consequently by an NMR line shape dominated by a relatively large quadrupolar coupling constant C_Q ($2.4 \leq C_Q \leq 2.9$ MHz). On the other hand, the B sites in the BO_4 tetrahedra are characterised by higher symmetry than those in BO_3 triangles. Consequently, the NMR line shapes of BO_4 sites are nearly Gaussian, resulting from small C_Q values (typically, $0 \leq C_Q \leq 0.5$ MHz). Moreover, the ^{11}B isotropic chemical shifts δ_{iso} of the BO_3 and BO_4 sites differ by $\sim$15–20 ppm [11]. These differences in C_Q and δ_{iso} of the BO_3 and BO_4 sites make them easily identifiable in the ^{11}B NMR spectra. Although, the δ_{iso} for each of these sites vary over a small range, recent detailed ^{11}B NMR studies of a wide variety of borate crystals have shown that at least in the case of BO_3 sites such variation can be empirically associated with the existence of structural systematics such as the number of bridging vs. non-bridging oxygen nearest neighbours and the sum of cation–oxygen bond strengths [11]. Recently available high-field ^{11}B NMR data have also shown the presence of chemical shift anisotropy (CSA) in BO_3 and BO_4 sites, although, precise experimental determinations of CSA and asymmetry parameter η_{CS} of the CSA remain experimentally challenging [11–13].

First-principles calculation of the NMR shielding tensor and quadrupolar coupling parameters C_Q and asymmetry parameter η_Q are extremely useful in understanding the correlation between atomic structure and NMR parameters and can be used to interpret the solid-state NMR spectra to the fullest extent. Such calculations in the past have been largely limited to molecular clusters of various sizes that were used to approximate various local structural environments in periodic solids [14–16]. First-principles calculations of NMR parameters in periodic solids have become feasible with the use of density functional theory (DFT) and the recently developed gauge-including projector augmented wave (GIPAW) method with plane-wave basis sets and pseudopotential approximation [17–20]. NMR shielding tensor parameters are obtained via calculation of the magnetic response of the all-electron wavefunction. We present here the results of such first-principles calculations of ^{11}B NMR parameters for a variety of borate crystal structures characterised by a range of B coordination environments (Table 1). These results agree well with the

*Email: sbsen@ucdavis.edu

ISSN 0892-7022 print/ISSN 1029-0435 online

DOI: 10.1080/08927020802258716
http://www.informaworld.com

Table 1. Composition and structural characteristics of the borate crystals studied in this work.

Chemical composition	Short-range structure	Superstructural ring units [Refs.]
1. B_2O_3	Two corner-linked BO_3 sites with all bridging oxygen atoms, B—O—B angles range between ~128–133°	None [19]
2. SrB_4O_7	Two highly asymmetric BO_4 units	None [20]
3. $LiBO_2$	One asymmetric BO_3 site with two bridging and one non-bridging oxygen	None [21]
4. $Mg_3B_2O_6$	One symmetric orthoborate BO_3 site with all non-bridging oxygen atoms	None [22]
5. CsB_3O_5	Two BO_3 and one BO_4 site with all bridging oxygen atoms forming a planar B_3O_7 triborate ring, in-plane B—O—B angles are ~120°	Triborate ring [23]
6. α-Li_3BO_3	One symmetric orthoborate BO_3 site with all non-bridging oxygen atoms	None [24]
7. α-$Cs_2B_{18}O_{28}$	Eight BO_3 and one BO_4 sites with all bridging oxygen atoms. Six BO_3 sites belong to two planar B_3O_6 boroxol rings while the other two BO_3 sites belong to a planar B_3O_7 triborate group, average in-plane B—O—B angles are ~120° in all cases	Boroxol and triborate rings [25]

available experimental data on these materials and provide fundamental underpinning of the empirical correlations between structure and experimental NMR parameters reported in the literature.

2. Calculation methodology

The DFT based codes CASTEP and CASTEP-NMR (Accelrys Inc., San Diego, CA, USA) were used for calculations of the ^{11}B NMR parameters for B sites in B_2O_3, $LiBO_2$, $Mg_3B_2O_6$, CsB_3O_5, α-$Li_3B_2O_3$, α-CsB_9O_{14} and SrB_4O_7 crystal structures [19,21–28]. The short-range structure around B atoms and the nature of the superstructural borate group in these materials are listed in Table 1. The unit cell parameters and atom positions for all crystal structures were taken from diffraction-based structural refinement studies published in the literature and were used for calculation of ^{11}B NMR parameters without further geometry optimisation [21–27]. The GIPAW algorithm and the generalised gradient approximation (GGA) simplified by Perdew–Burke–Ernzerhof functional were employed [17–20]. An energy cutoff of 600–650 eV was used for the plane wave basis expansions. The Brillouin zone was sampled using the Monkhorst–Pack scheme and a 4 × 3 × 3 *k*-point grid [19]. All core-valence interactions are modelled with ultrasoft pseudopotentials. Recent studies have demonstrated the excellent accuracy of the GIPAW method in calculating the NMR parameters for ^{29}Si,^{17}O, ^{25}Mg, ^{23}Na and ^{51}V nuclides in a variety of crystals and glasses [28–34]. These calculations yield the absolute shielding tensor principal components σ_{xx}, σ_{yy} and σ_{zz}. The isotropic chemical shift δ_{iso} was obtained from isotropic shielding $\sigma_{iso} = 1/3(\sigma_{xx} + \sigma_{yy} + \sigma_{zz})$ using the relationship: $\delta_{iso} = -(\sigma_{iso} - \sigma_{ref})$, where σ_{ref} is the isotropic shielding of a reference material. The calculated ^{11}B isotropic shielding of the BO_3 site in $LiBO_2$ crystal (78.03 ppm) has been used as a reference in this study and its δ_{iso} has been equated to the experimentally determined value of $\delta_{iso} = 17.08$ ppm [11]. The CSA and asymmetry parameter η_{CS} have been calculated using the relationships: CSA $= (\sigma_{zz} - \sigma_{iso})$ and $\eta_{CS} = (\sigma_{yy} - \sigma_{xx})/(\sigma_{zz} - \sigma_{iso})$. The principal components of the electric field gradient tensor V_{ii} are reported as C_Q and η_Q for enabling comparison with the experimentally determined values of these two parameters, where the relationships between V_{ii} and C_Q and η_Q can be expressed as: $C_Q = eQV_{zz}/h$ and $\eta_Q = (V_{xx} - V_{yy})/V_{zz}$. The convention $|V_{zz}| \geq |V_{yy}| \geq |V_{xx}|$ and the literature-reported quadrupole moment Q of 40.59 mB for ^{11}B were used [35].

3. Results and discussion

The calculated ^{11}B NMR parameters δ_{iso}, CSA,η_{CS}, C_Q and η_Q for all crystal structures are listed in Table 2. The δ_{iso}, C_Q and η_Q are the three NMR parameters that are most readily measured experimentally with ^{11}B NMR spectroscopy. The calculated values of these three parameters for all crystals are compared with the corresponding available experimental data in Table 2 and in Figures 1 and 2. The calculated values of δ_{iso}, C_Q and η_Q agree within ±0.7 ppm, ±0.08 MHz and ±0.05, respectively, in all cases.

It may be noted here that similar good agreement between theory and experiment has also been observed

Table 2. Calculated and experimental ^{11}B NMR parameters for BO_3 and BO_4 sites in different crystal structures.

Crystal [Refs. for NMR experiment]	Calculated ^{11}B NMR parameters						Experimental ^{11}B NMR parameters			
	δ_{iso} (ppm)	CSA (ppm)	η_{CS}	Ω (ppm)/κ	C_Q[a] (MHz)	η_Q	δ_{iso} (ppm)	Ω (ppm)/κ[b]	C_Q (MHz)	η_Q
B_2O_3 [11][c]										
BO_3-B1	14.50	11.68	0.95	23.07/0.04	2.661	0.15	14.6 ± 0.1[b]	15 ± 2/1.0	2.690 ± 0.005	<0.05
BO_3-B2	14.89	11.14	0.97	22.11/0.02	2.638	0.18				
SrB_4O_7										
BO_4-B1	0.49	−12.74	0.90	24.84/−0.08	1.149	0.42	n.a.	n.a.	n.a.	n.a.
BO_4-B2	0.14	12.25	0.51	21.50/0.42	0.677	0.70				
$LiBO_2$ [10,11]									2.47 [10]	0.50 [10]
BO_3-B1	17.08	43.58	0.90	84.98/0.08	2.552	0.54	17.08 ± 0.06	n.a.	2.56 [11]	0.60 [11]
$Mg_3B_2O_6$ [11]										
BO_3-B1	23.18	9.17	0.05	13.98 /0.93	2.863	0.05	22.5 ± 0.1	n.a.	2.94 ± 0.02	<0.05
CsB_3O_5 [5]										
TR-BO_3-B1	17.69	−18.95	0.91	37.05/−0.07	2.469	0.34	17.8	n.a.	2.55	0.30
TR-BO_3-B2	19.90	−18.16	0.67	33.32/−0.27	2.810	0.27	19.1	n.a.	2.75	0.27
BO_4 site	1.31	7.57	0.62	13.70/0.31	0.177	0.49	0.5	n.a.	0.17	0.50
α-Li_3BO_3 [10]										
BO_3-B1	21.25	−5.60	0.50	9.80/−0.43	2.687	0.05	n.a.	n.a.	2.64	0.035–0.048
α-$Cs_2B_{18}O_{28}$ [11][c]										
TR-BO_3-B2	16.80	−15.30	0.75	28.69/−0.20	2.539	0.32				
TR-BO_3-B3	16.76	−14.97	0.72	27.84/−0.23	2.535	0.33	16.7 ± 0.2[c]	21 ± 2/1.0	2.50 ± 0.05	0.2[b]
BR-BO_3-B4	16.52	13.28	0.83	25.43/0.13	2.509	0.54				
BR-BO_3-B5	16.75	14.53	0.81	27.68/0.15	2.533	0.14				
BR-BO_3-B6	17.00	14.21	0.76	26.70/0.19	2.547	0.22				
BR-BO_3-B7	16.61	13.80	0.79	26.15/0.17	2.523	0.55				
BR-BO_3-B8	17.23	14.46	0.76	27.18/0.19	2.589	0.21				
BR-BO_3-B9	17.45	14.68	0.73	27.38/0.21	2.640	0.09				
BO_4 site-B1	1.06	−5.2	0.46	9.00/−0.47	0.164	0.59	0.95	n.a.	0.20 ± 0.05	>0.50

Experimental values when not available are indicated by 'n.a.' 'TR' and 'BR' represents triborate and boroxol rings, respectively.[a] Absolute values are reported. [b] Value was fixed in experimental line shape calculation [11]. [c] Experimental values are reported as averages of multiple sites due to lack of spectral resolution [11].

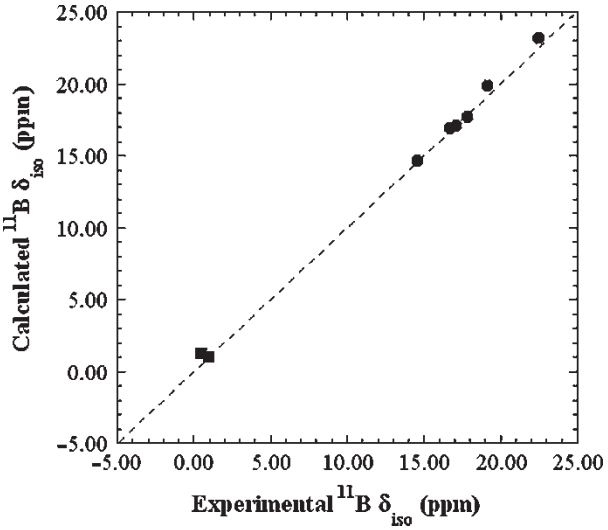

Figure 1. Comparison between the calculated and experimentally obtained ^{11}B δ_{iso} values for BO_3 (circles) and BO_4 (squares) sites in borate crystals. In case of B_2O_3 and $Cs_2B_{18}O_{28}$ the mean of the calculated δ_{iso} values for all BO_3 sites are compared with the experimentally determined average δ_{iso}. Dashed diagonal line through the plot represents the locus of all points with equal values of abscissa and ordinate.

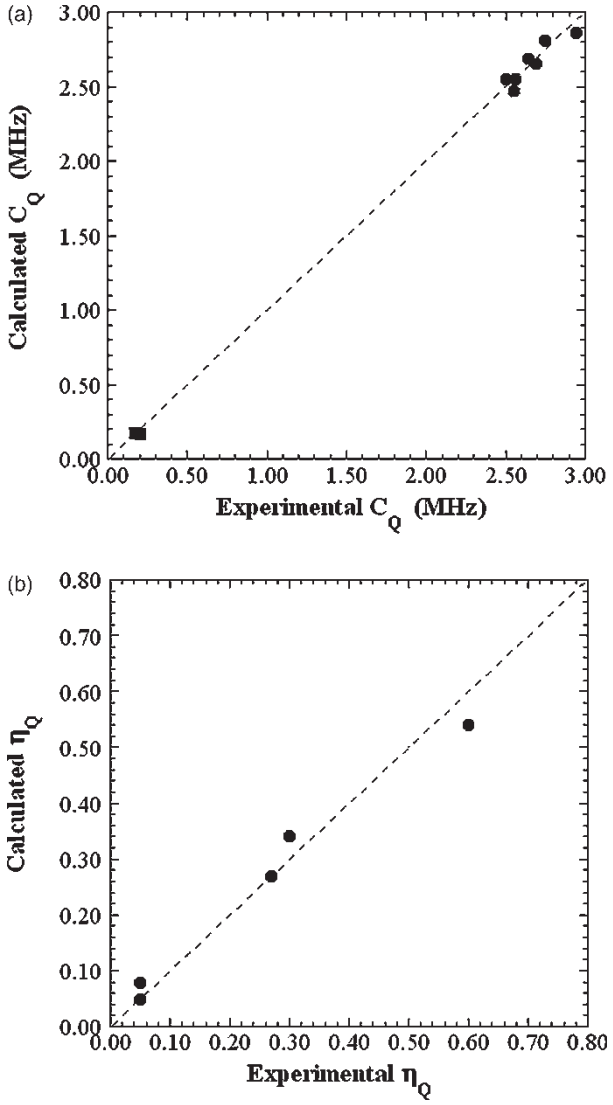

Figure 2. Comparison between the calculated and experimentally obtained (a) C_Q values for BO_3 (circles) and BO_4 (squares) sites and (b) η_Q values for BO_3 (circles) sites in borate crystals. In case of B_2O_3 and $Cs_2B_{18}O_{28}$ the mean of the calculated C_Q values for all BO_3 sites are compared with the experimentally determined average values. Calculated and experimental η_Q values for BO_3 sites in $Cs_2B_{18}O_{28}$ and for BO_4 sites in all crystals are not compared, since experimental values for these sites are not accurately known. Dashed diagonal line through each plot represents the locus of all points with equal values of abscissa and ordinate.

in a recent study based on DFT calculations of C_Q and η_Q values for B sites in a number of borate and borosilicate crystals [35].

In addition to δ_{iso}, C_Q and η_Q that are typically measured in NMR experiments on quadrupolar nuclides, these calculations also provide the principal values of the ^{11}B shielding tensor and hence the span of the shielding anisotropy Ω defined as: $\Omega = \sigma_{zz} - \sigma_{xx} = \delta_{xx} - \delta_{zz}$ [12]. The principal components of the chemical shift tensor are ordered such that $\delta_{xx} \geq \delta_{yy} \geq \delta_{zz}$ and therefore, Ω is always positive. The corresponding skew of the tensor is defined as $\kappa = 3(\delta_{yy} - \delta_{iso})/\Omega$. Experimental measurement of the parameter Ω for a quadrupolar nuclide such as ^{11}B is not common and it has recently become feasible with NMR spectroscopy at high magnetic fields of $\sim$14.1 T and higher [11]. A comparison of the calculated values of Ω with the available experimental data for this parameter for BO_3 sites in B_2O_3 and $Cs_2B_{18}O_{28}$ crystals shows somewhat poor agreement with the calculated values being significantly higher than the experimental values (Table 2). However, such a discrepancy may arise due to the approximations involved in obtaining Ω values from simulations of experimental central and satellite spinning sideband line shapes. For example, in the case of B_2O_3 crystal the small value of η_Q was taken as evidence for a similarly small value of η_{CS} and the shielding tensor was taken to be axially symmetric for the calculation of Ω [11]. However, the calculated ^{11}B NMR parameters for various BO_3 sites in Table 2 indicate the lack of any clear correlation between η_Q and η_{CS}. Therefore, caution should be exercised in making unwarranted assumptions to reduce the number of unknowns in the analyses of powder ^{11}B NMR data for both chemical shift and quadrupolar coupling tensor, since such analyses will always be underconstrained at a single magnetic field. The largest Ω value of $\sim$85 ppm is observed for BO_3 sites with a mixture of bridging and non-bridging oxygen atoms in $LiBO_2$ crystal and smaller Ω values ($\sim$22–37 ppm) are found to be characteristic of BO_3 sites with all three bridging

oxygen atoms in B_2O_3, CsB_3O_5 and $Cs_2B_{18}O_{28}$ (Table 2). The lowest Ω values ($\sim$10–14 ppm) are found for BO_3 sites with all three non-bridging oxygen atoms in Li_3BO_3 and $Mg_3B_2O_6$ (Table 2). This general trend is consistent with previous experimental results [11]. A similar trend is also observed for the variation of η_Q for the BO_3 sites in these crystal structures (Table 2).

The theoretically calculated Ω values for the BO_4 sites in CsB_3O_5 and $Cs_2B_{18}O_{28}$ are rather small ($\sim$9–14 ppm) and are comparable with the Ω values characteristic of BO_3 sites with all three non-bridging oxygen atoms (Table 2). Not surprisingly, the C_Q values for these BO_4 sites are also rather small (Table 2). This result is consistent with the regular site symmetry of these BO_4 tetrahedra characterised by maximum variation of B—O bond lengths of $\sim$0.03 Å for any tetrahedron [25,27]. The magnitude of the corresponding CSA values for these BO_4 sites is found to range between $\sim$5 and 8 ppm (Table 2). A recent high-field (14.1 T) ^{11}B NMR study has reported a similar range of CSA values for BO_4 sites in a number of borate and borosilicate crystals [13]. One interesting exception is the case of SrB_4O_7 crystal, where the two BO_4 sites are characterised by relatively large Ω and C_Q values (Table 2) that are consistent with the highly distorted nature of these two tetrahedra, where the maximum variation of B—O bond lengths are as high as $\sim$0.10–0.23 Å [22].

The ^{11}B δ_{iso} of BO_3 sites in borates have been shown in previous experimental studies to systematically increase with progressive replacement of bridging oxygen atoms with non-bridging oxygen atoms, as well as with decreasing cation–oxygen bond strength sum for all three O atoms bonded to a B atom [11]. However, a large variation in δ_{iso} ranging from 14.5 to up to 19.9 ppm has been observed in this study even for BO_3 sites with all three bridging oxygen atoms in three different crystal structures, namely, those of B_2O_3, CsB_3O_5 and $Cs_2B_{18}O_{28}$. Our calculations show that the ^{11}B δ_{iso} of non-ring BO_3 sites in B_2O_3 ranges between 14.5 and 14.9 ppm, while those of the BO_3 sites in three-membered triborate (B_3O_7) and boroxol (B_3O_6) type rings in CsB_3O_5 and $Cs_2B_{18}O_{28}$ are deshielded and range between 16.5 and 19.9 ppm (Table 2). It may be noted that BO_3 sites in triborate and boroxol rings are characterised by average B—O—B angles of $\sim$120° [25,27]. In contrast, the B—O—B angles in non-ring BO_3 sites in B_2O_3 are significantly larger ($\sim$128–133°; [21]). A previous DFT study of boroxol-ring and non-ring BO_3 sites in molecular clusters had suggested that such difference in B—O—B angles is responsible for the corresponding difference between the ^{11}B NMR parameters of boroxol ring and non-ring sites [14]. Interestingly, the δ_{iso} values for eight different BO_3 sites in triborate and boroxol rings in CsB_3O_5 and $Cs_2B_{18}O_{28}$, as determined in this study vary over a narrow range ($\sim$17–20 ppm) that is distinctly higher than the δ_{iso} for non-ring BO_3 sites in crystalline B_2O_3. This result clearly demonstrates that B—O—B angle may indeed be an important controlling factor for ^{11}B δ_{iso} of BO_3 sites with all three bridging oxygen atoms. On the other hand, the ^{11}B δ_{iso} for such sites in ring and non-ring configurations do not show any simple systematic correlation with the cation–oxygen bond strength sums, unlike the trend that has been previously observed experimentally for BO_3 sites with non-bridging oxygen atoms in crystalline borates [11]. For example, the cation–oxygen bond strength sums for the two BO_3 sites in CsB_3O_5 with $\delta_{iso} = 17.7$ and 19.9 ppm are 5.95 and 6.18, respectively, displaying an increasing trend of δ_{iso} with increasing cation–oxygen bond strength sum, which is the opposite of the decreasing trend observed in other borates [11]. It is also interesting to note in this regard that the CSA values of the BO_3 sites in the triborate rings are consistently negative while those for the BO_3 sites in boroxol-ring or non-ring geometries are consistently positive (Table 2).

High-field ^{11}B MAS NMR and ^{11}B dynamic-angle-spinning NMR studies of glassy B_2O_3 have shown the presence of two BO_3 sites with δ_{iso} $\sim$17.8 and 13.3 ($\pm$1.0) ppm that have been assigned to boroxol-ring and non-ring environments, respectively [14]. This assignment is fully consistent with the observed trend of deshielding of the ring BO_3 sites in CsB_3O_5 and $Cs_2B_{18}O_{28}$ structures with respect to the non-ring BO_3 sites in crystalline B_2O_3 (Table 2). It may be noted that within experimental error the ^{11}B δ_{iso} of the deshielded BO_3 site in glassy B_2O_3 agrees remarkably well with the rather tight range of chemical shifts ($\sim$16.5–17.5 ppm) obtained in this study, for the six different BO_3 sites in boroxol rings in crystalline $Cs_2B_{18}O_{28}$ (Table 2). Therefore, the boroxol-ring geometry in glassy B_2O_3 would have to be similar to those present in the structure of crystalline $Cs_2B_{18}O_{28}$.

4. Conclusions

The results of the present study demonstrate good agreement between the experimental ^{11}B NMR shielding and electric field gradient parameters and those obtained from first-principles calculations using DFT along with the GIPAW algorithm, for a wide variety of borate crystal structures. The calculated ^{11}B NMR parameters for various BO_3 sites indicate that the quadrupolar and chemical shielding asymmetry parameters η_Q and η_{CS} are largely uncorrelated. The ^{11}B δ_{iso} appears to be controlled by B—O—B angles for BO_3 sites with all three bridging oxygen atoms. This result is in contrast with the case for BO_3 sites with non-bridging oxygen atoms, where previous experimental studies have shown that ^{11}B δ_{iso} is controlled primarily by the number of non-bridging oxygen nearest neighbours and cation–oxygen bond strength sums. The characteristic ^{11}B δ_{iso} for BO_3 sites in boroxol ring geometries indicates that such rings in glassy B_2O_3 must be similar in geometry to those in crystalline $Cs_2B_{18}O_{28}$.

References

[1] Y. Mori, Y.K. Yap, T. Kamimura, M. Yoshimura, and T. Sasaki, *Recent development of nonlinear optical borate crystals for UV generation*, Opt. Mater. 19 (2002), pp. 1–5.

[2] E. Cavalli, D. Jaque, N.I. Leonyuk, A. Speghini, and M. Bettinelli, *Optical spectra of Tm^{3+}-doped $YAl_3(BO_3)_4$ single crystals*, Phys. Stat. Sol. C4 (2007), pp. 809–812.

[3] M. Cable and J. M. Parker, (eds), *High-Performance Glasses*. Chapman and Hall, New York, 1992.

[4] P.J. Bray, *NMR and NQR studies of boron in vitreous and crystalline borates*, Inorg. Chim. Acta 289 (1999), pp. 158–173.

[5] P.M. Aguiar and S. Kroeker, *Medium-range order in cesium borate glasses probed by double-resonance NMR*, Solid State NMR 27 (2005), pp. 10–15.

[6] R. Martens and W. Muller-Warmuth, *Structural groups and their mixing in borosilicate glasses of various compositions – an NMR study*, J. Non-Cryst. Solids 265 (2000), pp. 167–175.

[7] G.L. Turner, K.A. Smith, R.J. Kirkpatrick, and E. Oldfield, *Boron-11 nuclear magnetic resonance spectroscopic study of borate and borosilicate minerals and a borosilicate glass*, J. Magn. Reson. 67 (1986), pp. 544–550.

[8] G. Kunath-Fandrei, D. Ehrt, and C. Jäger, *Progress in structural elucidation of glasses by ^{27}Al and ^{11}B satellite transition NMR spectroscopy*, Z. Naturforsch. A: Phys. Sci. 50a (1995), pp. 413–422.

[9] S. Kroeker, S.A. Feller, M. Affatigato, C. O'Brien, W. Clarida, and M. Kodama, *Multiple four-coordinated boron sites in cesium borate glasses and their relation to medium-range order*, Phys. Chem. Glasses 44 (2003), pp. 54–58.

[10] D. Holland, S.A. Feller, T.F. Kemp, M.E. Smith, A.P. Howes, D. Winslow, and M. Kodama, *Boron-10 NMR: What extra information can it give about borate glasses?* Phys. Chem. Glasses 48 (2007), pp. 1–8.

[11] S. Kroeker and J.F. Stebbins, *Three-coordinated Boron-11 chemical shifts in borates*, Inorg. Chem. 40 (2001), pp. 6239–6246.

[12] D.L. Bryce, R.E. Wasylishen, and M. Gee, *Characterization of tricoordinate boron chemical shift tensors: Definitive high-field solid-state NMR evidence for anisotropic boron shielding*, J. Phys. Chem. A 105 (2001), pp. 3633–3640.

[13] M.R. Hansen, T. Vosegaard, H.J. Jakobsen, and J. Skibsted, *^{11}B chemical shift anisotropies in borates from ^{11}B MAS, MQMAS, and single-crystal NMR spectroscopy*, J. Phys. Chem. A 108 (2004), pp. 586–594.

[14] J.W. Zwanziger, *The NMR response of boroxol rings: A density functional theory study*, Solid State NMR 27 (2005), pp. 5–9.

[15] J.A. Tossell, *Calculation of the structural and spectral properties of boroxol ring and non-ring B sites in B_2O_3 glass*, J. Non-Cryst. Solids 183 (1995), pp. 307–314.

[16] J.A. Tossell, *Calculation of B and O NMR parameters in molecular models for B_2O_3 and alkali borate glasses*, J. Non-Cryst. Solids 183 (1997), pp. 236–243.

[17] F. Mauri, B.G. Pfrommer, and S.G. Louie, Ab initio *theory of NMR chemical shifts in solids and liquids*, Phys. Rev. Lett. 77 (1996), pp. 5300–5303.

[18] C.J. Pickard and F. Mauri, *All-electron magnetic response with pseudopotentials: NMR chemical shifts*, Phys. Rev. B 63 (2001), 245101.

[19] M.D. Segall, P.J.D. Lindan, M.J. Probert, C.J. Pickard, P.J. Hasnip, and S.J. Clark, *First-principles simulation: Ideas, illustrations and the CASTEP code*, J. Phys. Cond. Matt. 14 (2002), pp. 2717–2744.

[20] J.P. Perdew, K. Burke, and M. Ernzerhof, *Generalized gradient approximation made simple*, Phys. Rev. Lett. 77 (1996), pp. 3865–3868.

[21] G.E. Gurr, P.W. Montgomery, C.D. Knutson, and B.T. Gorres, *The crystal structure of trigonal diboron trioxide*, Acta Crystallograph. B26 (1970), pp. 906–915.

[22] A. Perloff and S. Block, *The crystal structure of the strontium and lead tetraborates, $SrO.2B_2O_3$ and $PbO.2B_2O_3$*, Acta Crystallograph. 20 (1966), pp. 274–279.

[23] A. Kirfel, G. Will, and R.F. Stewart, *The chemical bonding in lithium metaborate, $LiBO_2$. Charge densities and electrostatic properties*, Acta Crystallograph. B39 (1983), pp. 175–185.

[24] S.V. Berger, *The crystal structure of the isomorphous orthoborates of cobalt and magnesium*, Acta Chem. Scand. 3 (1949), pp. 660–675.

[25] J. Krogh-Moe, *Refinement of the crystal structure of caesium triborate, $Cs_2O.3B_2O_3$*, Acta Crystallograph. B30 (1974), pp. 1178–1180.

[26] F. Stewner, *Die Kristallstruktur von α-Li_3BO_3*, Acta Crystallograph. B27 (1971), pp. 904–910.

[27] N. Penin, M. Touboul, and G. Nowogrocki, *Refinement of α-CsB_9O_{14} crystal structure*, J. Solid State Chem. 175 (2003), pp. 348–352.

[28] S.E. Ashbrook, L. Le Polles, C.J. Pickard, A.J. Berry, S. Wimperis, and I. Farnan, *First-principles calculations of solid-state ^{17}O and ^{29}Si NMR spectra of Mg_2SiO_4 polymorphs*, Phys. Chem. Chem. Phys. 9 (2007), pp. 1587–1598.

[29] L. Truflandier, M. Paris, C. Payen, and F. Boucher, *First-principles calculations within periodic boundary conditions of the NMR shielding tensor for a transition metal nucleus in a solid state system: The example of V-51 in $AlVO_4$*, J. Phys. Chem. B 110 (2006), pp. 21403–21407.

[30] T. Charpentier, S. Ispas, M. Profeta, F. Mauri, and C.J. Pickard, *First-principles calculation of O-17, Si-29, and Na-23 NMR spectra of sodium silicate crystals and glasses*, J. Phys. Chem. B 108 (2004), pp. 4147–4161.

[31] E. Balan, F. Mauri, C.J. Pickard, I. Farnan, and G. Calas, *The aperiodic states of zircon: An* ab initio *molecular dynamics study*, Amer. Mineral. 88 (2003), pp. 1769–1777.

[32] I. Farnan, E. Balan, C.J. Pickard, and F. Mauri, *The effect of radiation damage on local structure in the crystalline fraction of $ZrSiO_4$: Investigating the ^{29}Si NMR response to pressure in zircon and reidite*, Amer. Mineral. 88 (2003), pp. 1663–1667.

[33] S. Rossano, F. Mauri, C.J. Pickard, and I. Farnan, *First-principles calculation of O-17 and Mg-25 NMR shieldings in MgO at finite temperature: Rovibrational effect in solids*, J. Phys. Chem. B 109 (2005), pp. 7245–7250.

[34] A. Soleilhavoup, M.R. Hampson, S.J. Clark, J.S.O. Evans, and P. Hodgkinson, *Using ^{17}O solid-state NMR and first principles calculation to characterise structure and dynamics in inorganic framework material*, Magn. Reson. Chem. 45 (2007), pp. S144–S155.

[35] M.R. Hansen, G.K.H. Madsen, H.J. Jakobsen, and J. Skibsted, *Refinement of borate structures from ^{11}B MAS NMR spectroscopy and density functional theory calculations of ^{11}B electric field gradients*, J. Phys. Chem. A 109 (2005), pp. 1989–1997.